Digital Object Identifier (DOI): 10.1109/TPEL.2017.2658182

IEEE Transaction on Power Electronics (Volume: 32, Issue: 12, Dec. 2017)

Power routing for cascaded H-Bridge converters

Youngjong Ko
Markus Andresen
Giampaolo Buticchi
Marco Liserre

Suggested Citation

Y. Ko, M. Andresen, G. Buticchi and M. Liserre, "Power Routing for Cascaded H-Bridge Converters," in *IEEE Transactions on Power Electronics*, vol. 32, no. 12, pp. 9435-9446, Dec. 2017.

Power Routing for Cascaded H-Bridge Converters

Youngjong Ko, *Student Member, IEEE*, Markus Andresen, *Student Member, IEEE*, Giampaolo Buticchi, *Member, IEEE*, and Marco Liserre, *Fellow, IEEE*

***Abstract*—Modular power converters are expected to play a major role in medium- and high-voltage/power applications. Normally, each module processes the same amount of power; however, this does not take into consideration that different modules can have a different remaining useful lifetime. This paper proposes the concept of power routing for cascaded H-bridge (CHB) converters, with the purpose of delaying the failure of the system. A third-harmonic injection into the duty cycles allows extending the imbalance capability of the structure, keeping the CHB operational even if some power paths are completely unloaded. Analytic investigation in conjunction with simulation and experimental measurements demonstrate the power routing by means of the proposed method.**

***Index Terms*—Active thermal control, cascaded H-bridge (CHB), multilevel converter, power routing, reliability.**

I. Introduction

POWER electronics are emerging in the medium-voltage range with application to medium-voltage drives or medium-voltage converters [1]. Due to the limitation of the blocking voltage and the high switching losses of the high-voltage semiconductors, the consolidated topologies such as the two-level voltage-source converter are impractical for medium-voltage applications. A possible solution is modular power converters composed of basic cells, which are splitting the required voltage, while the power semiconductors only need to be rated for the cell voltage. The cascaded H-bridge (CHB) converter has been applied to medium-voltage drives and proposed for grid-connected applications [1], [2]. The dc-link voltage of the CHB cells is fed by dc power supplies, which represent different power paths in the system. To the current state, they are equally loaded to balance the components stress with the implementation of special controls [3]. Unbalanced loading has been investigated for different voltage ratings in the cells [4] and was proposed for improved converter cell balancing with integrated cell storage by utilization of the third-harmonic component [5], [6].

Manuscript received July 14, 2016; revised November 4, 2016 and December 16, 2016; accepted January 13, 2017. Date of publication January 25, 2017; date of current version August 2, 2017. This work was supported in part by the European Union/Interreg V-A—Germany-Denmark, under PE:Region Project and in part by the European Research Council under the European Union's Seventh Framework Programme (FP/2007-2013)/ERC under Grant Agreement 616344—HEART. This paper was presented in part at the IEEE Energy Conversion Congress and Exposition, Milwaukee, WI, USA, September 18–22, 2016. Recommended for publication by Associate Editor M. Saeedifard.

The authors are with the Chair of Power Electronics, Christian-Albrechts University of Kiel, Kiel 24118, Germany (e-mail: yoko@tf.uni-kiel.de; ma@tf.uni-kiel.de; gibu@tf.uni-kiel.de; ml@tf.uni-kiel.de).

Color versions of one or more of the figures in this paper are available online at http://ieeexplore.ieee.org.

Digital Object Identifier 10.1109/TPEL.2017.2658182

Fault tolerant strategies have been adopted to bypass the damaged cells in the case of a failure [7]; however, instead of simply isolating the problem, it is possible to apply the physics of failure concept and optimize the system operation accordingly. A study investigating the failure's cause for power semiconductors has identified the manufacturing processes to be a source [8]. This results in a standard deviation in the quality of the components, which leads to different lifetimes. In addition, several failure mechanisms, such as the junction temperature dependent failures of power semiconductors, are dependent on the power processed by the cells. As a solution to optimize the operation of the CHB, the cells can be loaded depending on the condition of the components in the corresponding power path. The purpose is to avoid or delay as much as possible the failures dependent on the cell's processed power, shifting the load from the cells with older components. This is referred to the concept of active thermal control by means of power routing [9]. The condition of the components can be monitored [10], [11] and the loading is distributed accordingly, whereby components with a shorter remaining useful lifetime are unloaded. In this way, the power-dependent failures in the power paths connected to the CHB cells are delayed.

In this work, the power routing for the CHB converter is proposed to control the loading of the power paths. To increase the power-routing capability, the concept of multifrequency power routing is applied, by utilizing a third-harmonic voltage. The full output voltage reserve is demonstrated to be obtained even in case of a completely unloaded power supply. The concept of the third-harmonic component for power routing is analyzed theoretically and experimentally. Measurements on a seven-level CHB converter prototype are presented to validate the control of the power semiconductor's stress in the different power paths.

In Section II, the power routing is motivated, and in Section III, the concept is explained. Section IV investigates the unbalanced power-routing potential of the algorithm and the impact on the lifetime of the power semiconductors in the power paths. An experimental validation is demonstrated in Section V before this paper is concluded in Section VI.

II. Power Routing in CHB Converters

In the following, failure mechanisms for power semiconductors are reviewed. Furthermore, the motivation is given to transfer different power in the dc/dc converters of the CHB converter, as shown in Fig. 1.

A. Reliability in Power Converters

The reliability analysis of a system needs to use a physics of failure approach [12], and based on this approach, every failure

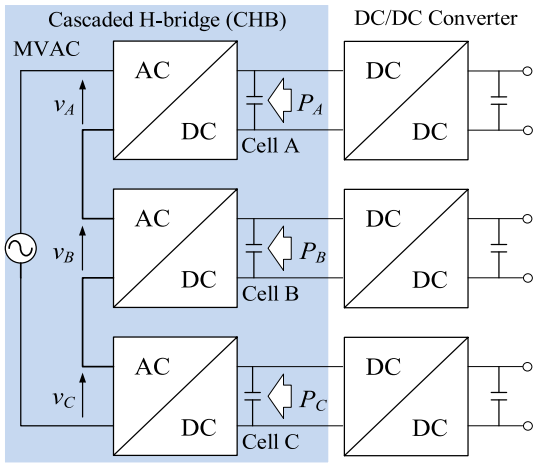

Fig. 1. Single phase of a CHB converter connected to dc/dc converters.

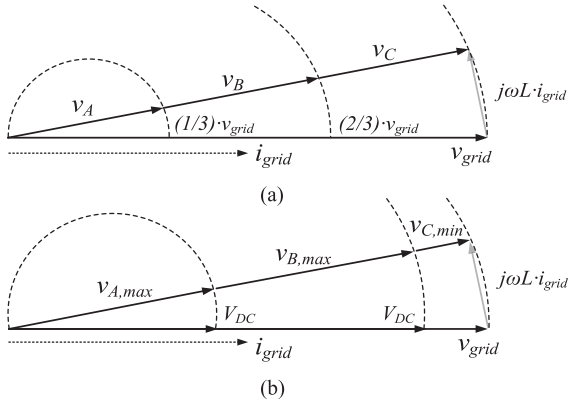

Fig. 2. Power imbalance by using the conventional fundamental voltage method. (a) Balanced power and (b) maximum unbalanced power loading.

of a component needs to be traced back to its physical mechanisms. In power converters, it has been found, that power semiconductors and capacitors are among the components, which fail most frequently [13]. Remarkably, most of their reported failure mechanisms are dependent on the power transfer and most failure mechanisms for the power semiconductor are related to thermal cycling, which is the heating up and cooling down of the power semiconductors. This causes failures such as bond wire lift off, baseplate solder fatigue and others [14]. The lifetime of power semiconductors is commonly expressed by the number of thermal cycles to failure N_f in dependence on the thermal swing ΔT_j and the average junction temperature $T_{j,\mathrm{mean}}$, of which the power semiconductor undergoes. This is shown in the following equation:

$$N_f = a_1 \cdot (\Delta T_j)^{-a_2} \cdot e^{\frac{a_3}{T_{j,\mathrm{mean}}}}. \tag{1}$$

In this equation, $a_2 \approx 5$ that results in a major influence for the lifetime[15], while a_1 is the linear influence of the power cycling capability and a_3 is the influence of the Arrhenius equation. The failure mechanisms for the capacitors are mostly related to the ripple current, affecting a temperature increase [16]. In order to reduce the stress, the ripple current, consequent to the power on a capacitor, needs to be reduced. However, in the following, the reliability of power semiconductors is put in focus

$$T_j = T_C + R_{\mathrm{th,JC}} \cdot P_{\mathrm{loss}}. \tag{2}$$

Common approaches for increasing the reliability of power semiconductors are an improved design with increased robustness or an overrating of components (e.g., current rating or cooling system). Another concept is to reduce the thermal cycles in magnitude or number of occurrences by means of software, which refers to active thermal control [17]. The application of active thermal control requires the knowledge of the junction temperature, which is usually hard to obtain during normal operation of the converter. However, in stationary conditions, the junction temperature of a power semiconductor T_j can be expressed with (2), whereby T_C represents the case temperature, $R_{\mathrm{th,JC}}$ the thermal resistance between junction and case, and P_{loss} the losses of the power semiconductors.

According to this equation, the thermal swing of the junction temperature is solely dependent on the losses and the ambient temperature, whereas the thermal resistance is constant. The case temperature settles in dependence of the junction temperature and the thermal properties of the cooling path. The most important influencing factor, the losses, are dependent on the voltage and the currents in the operation point and thus can be controlled by controlling the power transfer in the cells. As a consequence of controlling the power in one cell, the remaining cells need to share the variation of the power.

Among the solutions for increasing the reliability, active thermal control is the only method, which does not come for increased costs in the system design, while the robust design and overrating of components usually do increase the costs. However, the currently documented active thermal control algorithms bring disadvantages, such as lower efficiency or higher output current ripple.

B. Motivation for Power Routing

Several techniques for the power balancing of cells in modular power converters have been proposed and developed in order to share the stress identically [18]. These algorithms rely on the sharing of the fundamental voltage among multiple CHB cells or employ advanced balancing schemes embedded in the modulator without an external control loop [19]. In contrast to these approaches, the power routing proposed in this paper targets to unbalance the power in the system in order to control the loading of the power paths.

In the similar way to the power balancing method, the fundamental voltage among multiple CHB cells can achieve the designated unbalanced power routing, but offers a limited capability, which is heavily dependent on the ratio between dc-link voltage and converter output voltage. This is demonstrated for balanced condition in Fig. 2(a) and for unbalanced condition in Fig. 2(b). In addition to this limitation, due to efficiency reasons, the dc-link voltage margins should be designed as low as possible. Therefore, in order to overcome the limitation of the

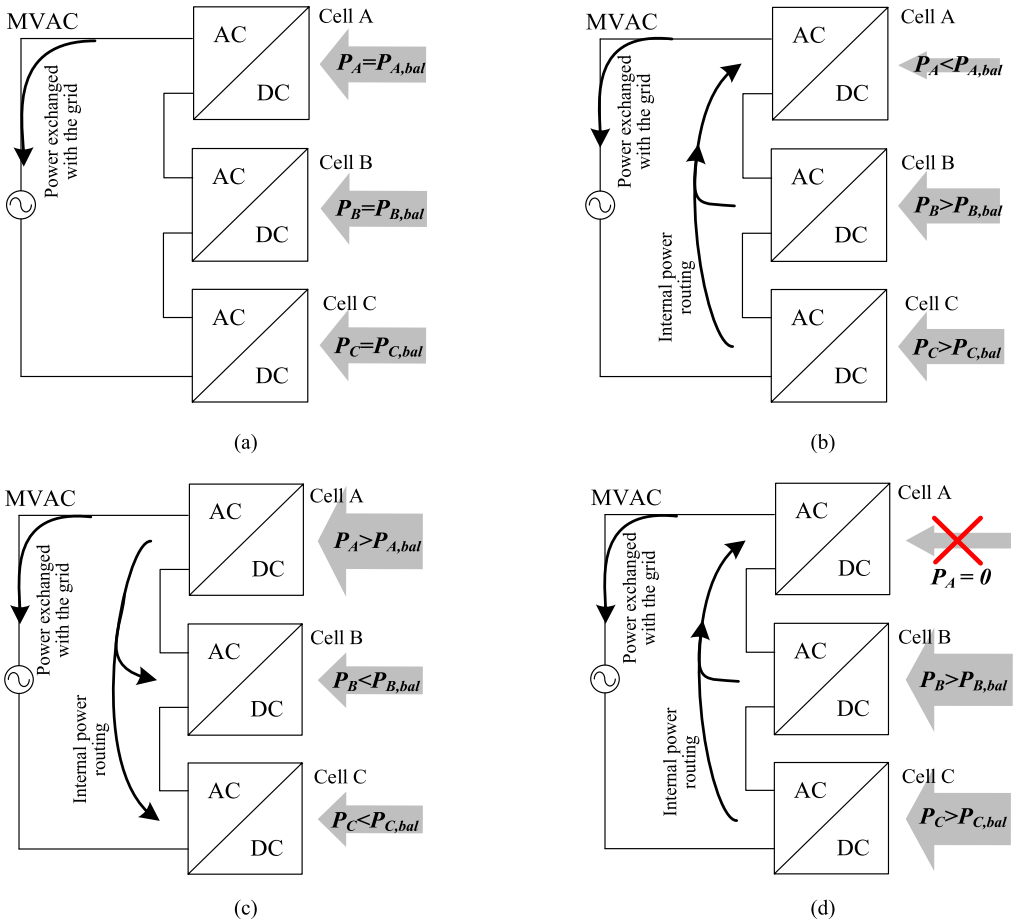

Fig. 3. Power flow between CHB cells by multifrequency method in case of (a) balanced loading, (b) unloading cell A, (c) overloading cell A, and (d) no power transfer into cell A.

conventional fundamental voltage, the multifrequency power routing using the third-harmonic voltage is proposed.

The proposed method is exploiting the third harmonic in order to improve the dc-link voltage utilization in a similar fashion to the Third-Harmonic injected sinusoidal pulse width modulation (SPWM) [20].

In order to implement the power routing, other methods for further extending the linear range of CHB converters could also be adopted [21]–[23]. Since the choice of the range extension technique does not alter the fundamental objective of the proposed approach, in the following, the third-harmonic injection will be used, due to the ease of implementation and fast open-loop operation. The adoption of more complex modulation techniques to further improve the thermal balancing capability represents nevertheless a possibility.

As pointed out in the last section, active thermal control can be applied to increase the reliability and power routing, in particular, for the application in modular converters. This targets to reduce the stress for aged parts in the system and to stress more on the less aged parts. The application of active thermal control brings advantages to the system, if the remaining lifetime among the components is different, which is already expected due to the high number of components in the system and imperfect manufacturing processes [24]. Other possible reasons for different remaining lifetimes can be the replacement of cells or the occurrence of events during operation, which cause damage only to some parts, while others are unaffected. In order to obtain the information about the remaining lifetime for the cells of the converter, condition monitoring is a possible solution. Measuring parameters such as the collector emitter voltage of IGBTs or the ON state resistance of MOSFETs enables to identify the wear-out of the power semiconductors [10]. However, for effectively applying active thermal control, the knowledge of the junction temperature is required and can be accessed by measurement with thermosensitive electrical parameters, observers, or estimators [25].

As an example, the CHB converter in Fig. 1 has three cells with three power paths (P_A, P_B, and P_C) and the components in one of the dc/dc converters show far higher degradation than the others. Since the converter is dependent on the operation of all cells, a failure of the one cell or power path is the end of life. Instead of loading the cells equally with a balanced power ($P_{A,\mathrm{bal}}$, $P_{B,\mathrm{bal}}$, and $P_{C,\mathrm{bal}}$), [as shown in Fig. 3(a)], unloading the power path with the highest degradation postpones the time to the failure, which is demonstrated in Fig. 3(b) for unloading path A. As the opposite concept, it is possible to load one path higher and to bring it close to its wear-out. This might be a solution, if the next maintenance is scheduled and the path is

planned to be replaced, while the remaining ones will not be replaced. This case is visualized in Fig. 3(c).

The case of completely unloading the power path connected to a CHB cell is shown in Fig 3(d). This might be mandatory, if a cell is not anymore able to exchange energy in this power paths. In order to implement the unbalanced power routing method, it should be assumed that the dc-link voltage is regulated by dc/dc converters. However, for continued operation after a fault in a dc/dc converter, the dc-link voltage needs to be controlled by the CHB converter at the expense of reduced power-routing capability.

III. Concept of the Multifrequency Power Routing

The concept of multifrequency power routing is introduced for the seven-level CHB converter in the architecture of Fig. 1. It is important to note that the basic principle can be extended to a greater number of cells, always improving the dc-link voltage utilization for power imbalance among the cells. In order to maximize the dc-link voltage utilization, the optimal magnitude of the third harmonic is derived in the following and holds high similarity to the mathematical derivation in [20]. The modulation function with additional third harmonic in dependence of the angle φ and the modulation index M is shown in the following equation:

$$m = M \cdot \cos(\varphi) + M \cdot k \cdot \cos(3 \cdot \varphi)). \tag{3}$$

Similar to the third-harmonic injection, the minimum magnitude is obtained for $k = -1/6$, leading to the maximum of the modulation function $m_{\max} = \sqrt{3}/2$. This enables to utilize the linear range of the converter cells up to the inverse of $m_{\max}$, which is $M = 1.155$. Of course, the power reduced with the third harmonic of one cell, needs to be provided by the other cells, which requires them to add the opposite harmonic sequence to their modulation function.

For the demonstration of the concept, Fig. 4 shows the unbalanced power sharing among three cells by means of the multifrequency power-routing method, where from the first to the third row are the duty cycle of three cells, A, B, and C, respectively. The last row shows the output power with respect to each cell. Since the duty cycle is typically normalized by the dc-link voltage, it is used instead of the actual voltage value in the figure. In the first column, the three cells share equal power, i.e., balanced power routing, with the same duty cycles. For the unbalanced power routing, the duty cycle of the overloaded cells increases while that of the unloaded cell decreases. As depicted in the second column, the unbalanced power routing by the fundamental voltage is restricted when two of the three duty cycles reach the maximum duty cycle. In order to achieve an even higher power imbalance, the third-harmonic voltage is utilized, which is in phase with the fundamental voltage as shown in the third column. For the overloaded cells, the third-harmonic voltage is added to the fundamental voltage so that the fundamental voltage utilizes the maximum linear range of $M = 1.155$. The fundamental voltage of the unloaded cell is reduced and it is absorbing the third-harmonic voltage from the overloaded cells.

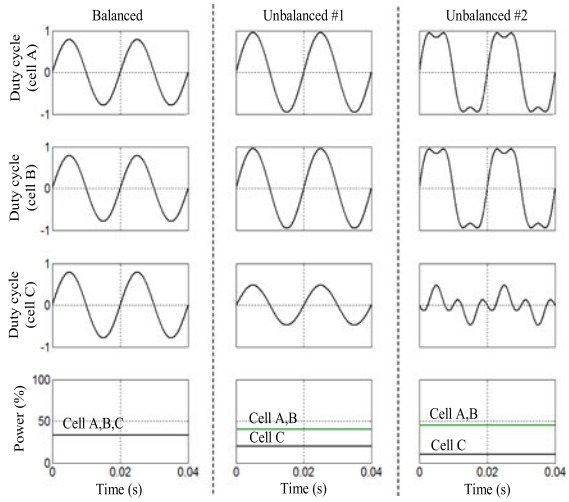

Fig. 4. Principle of imbalance power routing by a multifrequency method: Balanced is equal loading of all devices, Unbalanced #1 is unloading cell C with the fundamental voltage and Unbalanced #2 is unloading cell C with a multifrequency method.

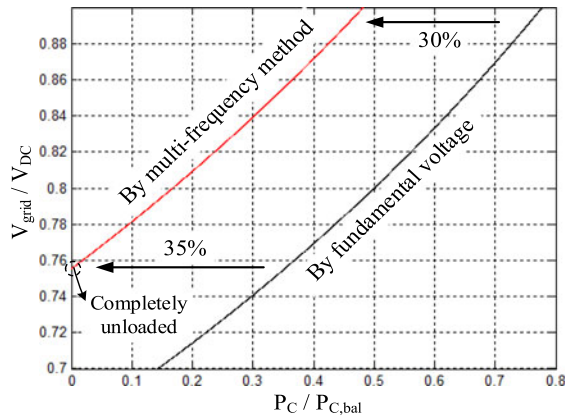

Fig. 5. Capability of unloading power depending on the ratio between grid voltage V_{grid} and dc-link voltage V_{DC}.

IV. Potential of the Multifrequency Method

In the following section, the potential of the power-routing capability is benchmarked in terms of the maximum potential power imbalance. The effect of power routing on the total harmonic distortion (THD) of the output current and the capacitor voltage ripple is analyzed. An example for controlling the stress in the power paths is given.

A. Potential of Power Imbalance

For demonstration of the power routing potential,Fig. 5 shows the maximum capability to unload a cell in dependence of the ratio between dc-link voltage and grid voltage, where the P_C presents the currently loaded power and the $P_{C,\mathrm{bal}}$ is the loaded power at balanced condition. As pointed out before, this ratio is commonly minimized in the converter design in order to achieve the required voltage reserve, but to optimize losses at the same time. However, it is shown that by means of the multifrequency method, the capability of power imbalance can be improved by at least 30%.

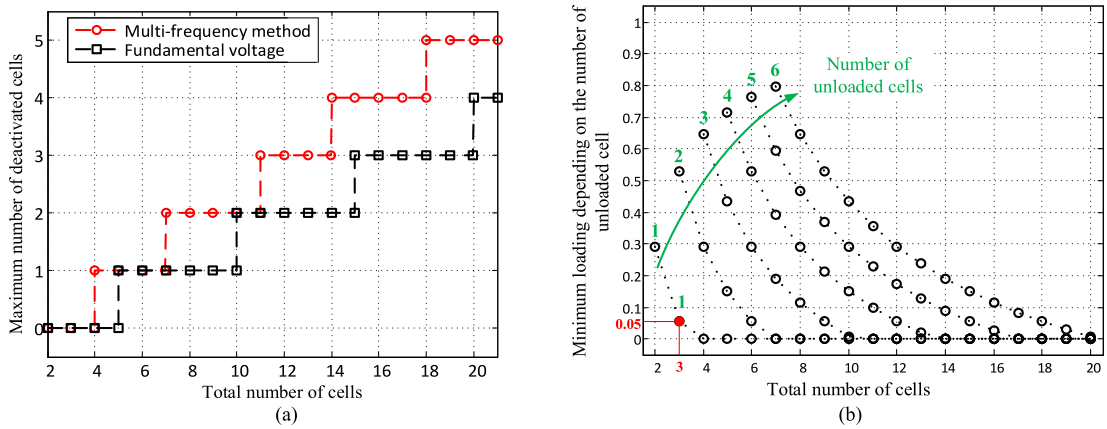

Fig. 6. Unloading cells potential depending on the total cell number for $V_{\mathrm{grid}}/V_{\mathrm{DC}} = 0.8$: (a) Comparison with/without multifrequency power routing (b) minimum loading depending on the number of unloaded cell.

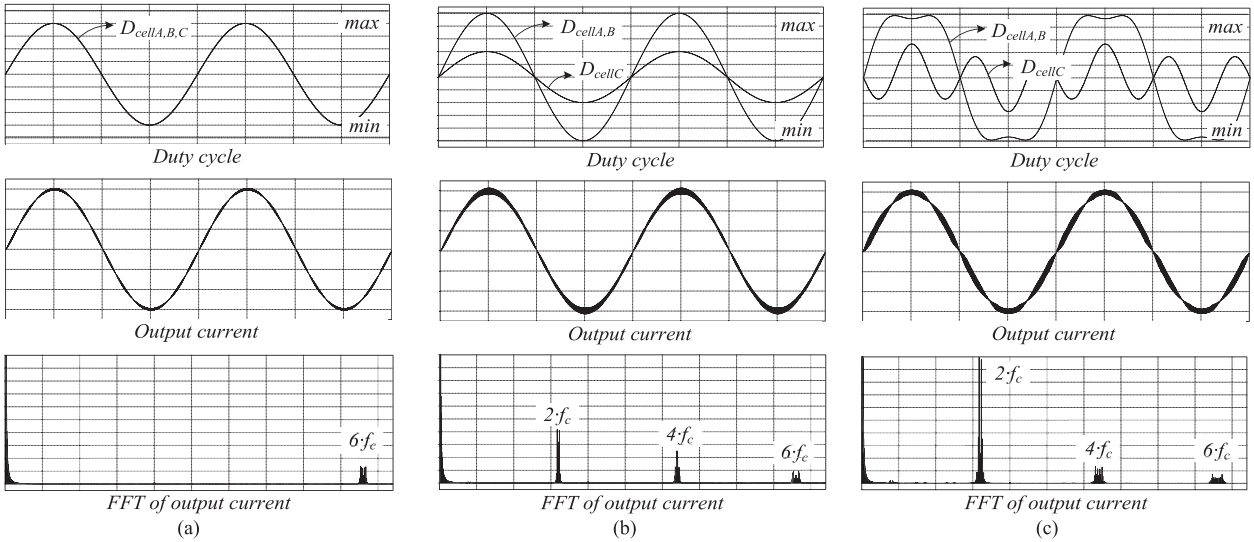

Fig. 7. Output current analysis in case of $V_{\mathrm{grid}}/V_{\mathrm{DC}} = 0.8$ showing the duty cycles, the output current, and its frequency spectrum: (a) for balanced conditions, (b) unloading cell C with the fundamental voltage, and (c) unloading cell C by means of multifrequency method.

Beside the ratio between dc-link voltage and grid voltage, the number of CHB cells has a major impact on the potential maximum power imbalance. In Fig. 6(a) the capability for completely unloading cells is presented with and without multifrequency power routing. The ratio between grid voltage and dc-link voltage is chosen to $V_{\mathrm{grid}}/V_{\mathrm{DC}} = 0.8$ and it can be seen, that a higher number of cells enable a higher potential power imbalance. Four cells are required as a minimum for completely unloading a power path with the multifrequency method, whereas five are required without the method. The power routing with the third harmonic is always superior to the case with only the fundamental voltage and for 19 cells; it enables to unload two cells more than that without the algorithm. Completely unloading a power paths is an extreme case, which is not always likely to be the optimal choice and it is more likely, that there is a number of cells, which need to be unloaded. This case is demonstrated in Fig. 6(b). The number of unloaded cells is demonstrated in the curves in dependence of the number of CHB cells on the *x*-axis. On the *y*-axis, the minimum power, which needs to be processed in the unloaded cells, is shown for this case. As an example (indicated in red), one cell in a CHB converter with three cells needs to be unloaded. This still requires to transfer 5% of the power in the unloaded cell, while the two other cells need to process the remaining 95% of the power.

B. Impact on the Current THD and the Capacitor Voltage Ripple

The third-harmonic voltages are canceling out themselves within the CHB converter cells as expressed in (4), where $v^*_{A,3}$ is the third-harmonic component of cell A, $v^*_{B,3}$ is the third-harmonic component of cell B, and $v^*_{C,3}$ is the third-harmonic component of cell C

$$v^*_{A,3} + v^*_{B,3} + v^*_{C,3} = 0. \tag{4}$$

However, these reference voltages are average values and the real converter output voltage is affecting the THD of the output current as shown in Fig. 7, where f_c is the carrier frequency. The duty cycles, the converter output current, and its frequency

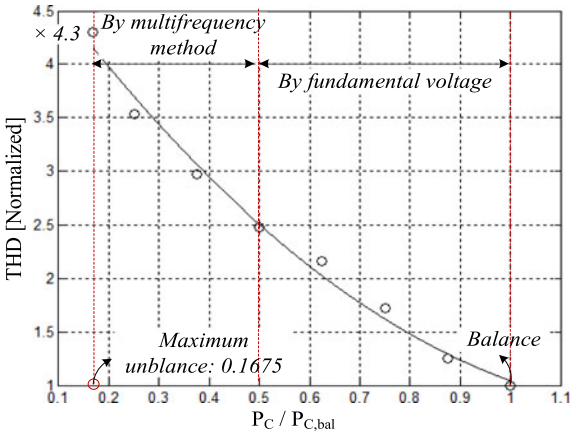

Fig. 8. THD of the output current for increasing imbalance of the power loading in the CHB converter normalized on the balanced conditions.

spectrum are shown. In Fig. 7(a), these are shown for the balanced loading and only the sixth-harmonic component exists in the current spectrum. This feature is the advantage of the phase-shifted carrier modulation with equal dc-link voltage and same duty cycles for each cell. The unbalanced power routing with the fundamental voltage is shown in Fig. 7(b), where the current ripple is higher compared to the first case, because the second and the fourth harmonics exist due to the duty cycles mismatch. In the third case [see Fig. 7(c)], the multifrequency method is applied, which can be seen in the duty cycles. The current ripple is increased and in the spectrum, the second-harmonic component is now highly increased.

A demonstration of the dependence between THD and the power imbalance in the CHB converter is shown in Fig. 8 in case cell A and B are additionally loaded and cell C is unloaded. For the maximum imbalance, the current THD is 4.3 times higher than in the balanced conditions. As a conclusion, the THD performance decreases with the imbalance due to the increased second and fourth harmonics as shown in Fig. 7, even though the third-harmonic component is completely compensated among the cells connected in series as (4).

The multifrequency method is also affecting the voltage ripple of the capacitors. For this reason, the voltage ripple of the balanced case [see Fig. 9(a)] is compared with the case of the multifrequency power routing in Fig. 9(b) and (c) for the overloaded cell and the unloaded cell, respectively. It can be seen, that the periodicity of the ripple is twice the grid frequency for all cases, but in case of an unloaded cell, a component at four times the grid frequency appears. The maximum deviation of the dc-link voltage is 0.6 V for all the three cases. The high-frequency ripple on the envelope of the voltage ripple is reduced for the overloaded cell and increased for the unloaded cell. Also, it can be seen that the envelope of the unloaded cell is having a higher peak-to-peak value. Since the capacitor current is the derivative of the capacitor voltage, compared to the balanced case, the current ripple is lower for the overloaded cell and higher for the unloaded cell. Consequently, the stress for the capacitor is increased for the unloaded cell, while it is reduced for the overloaded cell.

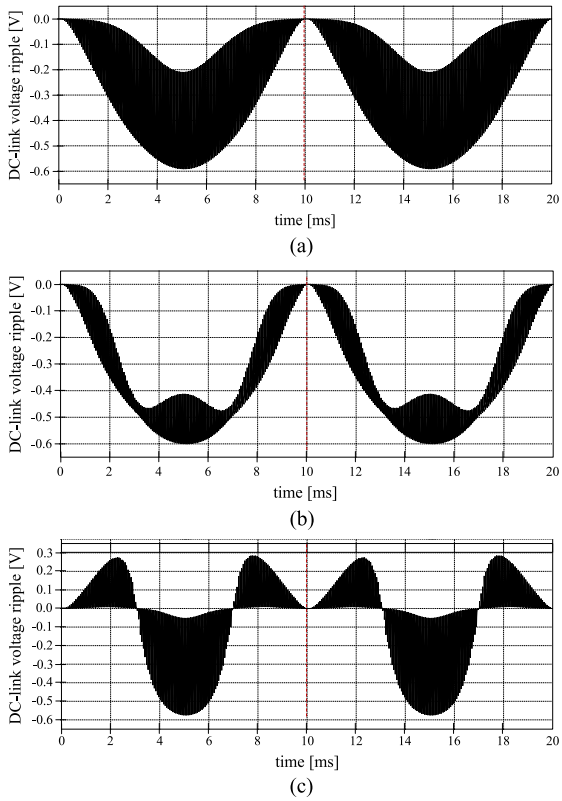

Fig. 9. DC-link voltage ripple in case of $V_{\mathrm{grid}}/V_{\mathrm{DC}} = 0.8$. (a) For the balanced case, (b) for the overloaded cell, and (c) for the unloaded cell by the multifrequency method.

C. Impact on the Power Semiconductors in the CHB Cells

In this paragraph, the loss distribution among the power semiconductors in the CHB cell is analyzed, depending on the balanced power loading. It is assumed, that cell A and B are additionally loaded and cell C is unloaded as an example. However, despite an imbalance in the power loading, every cell needs to contribute to the power loading—either with IGBTs or with freewheeling diodes. Consequently, the stress is redistributed without achieving an overall advantage for all power semiconductors of one CHB cell.

For the demonstration of the loss distribution, the discrete IGBTs (IXYH75N65C3H1) are used in the simulations. The loss distribution among IGBTs and diodes is shown for $V_{\mathrm{grid}}/V_{\mathrm{DC}} = 0.8$ in the cells with increased power in Fig. 10(a) and reduced power in Fig. 10(b), where the P_C presents the currently loaded power and the $P_{C,\mathrm{bal}}$ is the loaded power at balanced condition. In dependence on the design of the diode and the IGBTs, the efficiency is increasing or decreasing in case of the power routing. The characteristics of the diodes in the simulated power semiconductors present lower reverse recovery losses and lower conduction losses than the switching and conduction losses of the IGBTs, which is why the total losses in the unloaded cells decrease slightly, while the total losses in the overloaded cells are increasing. Also demonstrated is the variation of the losses in the diode/IGBT affected by the power routing. Additionally, the limitation of the power-routing capability with the

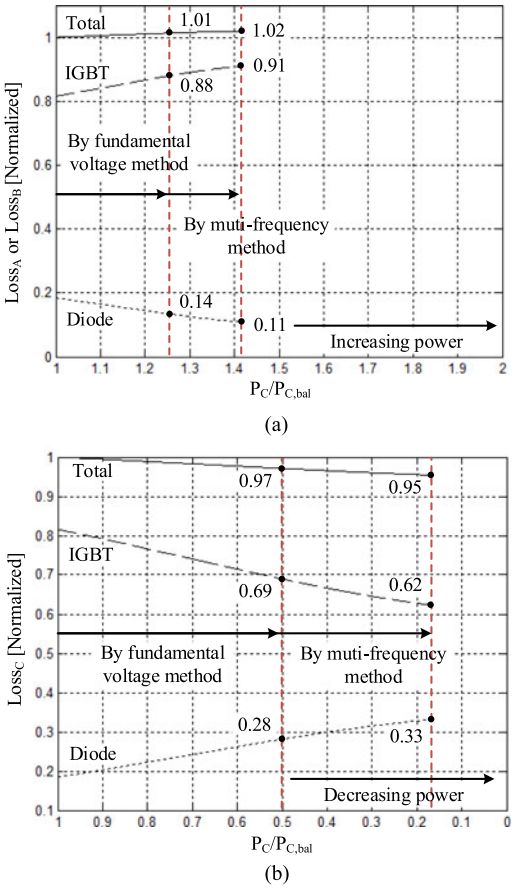

Fig. 10. Loss distribution of power semiconductors in CHB cell for $V_{\rm grid}/V_{\rm DC} = 0.8$. (a) Additionally loaded cell (Cell A or Cell B) and (b) unloaded cell (Cell C).

fundamental voltage is highlighted, showing the increased power-routing potential of the multifrequency method.

As a consequence, the power routing has not only an impact on the components in the corresponding power paths, but also on the stress distribution between IGBT and diode in the CHB cells. Thus, not only the degradation of the dc/dc converters can be considered, but also the stress distribution among the IGBTs/diodes in the CHB cells. Here, the targets of stress reduction for the dc/dc converter and the power semiconductors in the CHB cell can either be complementary or lead to a conflict of objectives.

D. Power Routing for Wear-Out Control

Based on the system in Fig. 1, the CHB cells can control the power transfer in the single dc/dc converter, which is utilized in order to unload the power paths. The implementation of the power routing is achieved with an additional open-loop control nested in the standard current controller, as shown in Fig. 11(a). The fundamental components are determined depending on the power reference, and the second constraint is the cancellation of the third harmonic for the multifrequency method in (4).

The flow chart of the proposed method is shown in Fig. 11(b), where the case that only one cell needs to be unloaded is considered for the sake of simplicity. When the reference power of each cell is different, the unbalanced power routing is activated and it is determined whether the multifrequency method should be applied or not, depending on the fundamental reference (v^*_{A1}, v^*_{B1}, v^*_{C1}). The multifrequency method is applied when one of the fundamental references exceeds the maximum modulation index. In this situation, proper third harmonics are determined with the optimized k in chapter III ($k = 1/6$). For instance, the negative third harmonics is added in cell A in order to unload its power while other cells employ the positive third harmonics divided by the number of overloaded cells N.

In Fig. 12, the power-routing concept is presented in a case study under consideration of the power-routing limitations highlighted in Fig. 6(b). A mission profile with rapidly fluctuating power is presented and the multifrequency power routing is applied to control the loading, particularly preventing power fluctuations in path one. A converter designed for an ambient temperature $T_a = 40\,^\circ$C and the maximum junction temperature $T_{j,\max} = 90\,^\circ$C under full load is assumed. The power-routing results in a reduced thermal fluctuation on the power semiconductors in that path, while the fluctuations in the other paths are increased. As a result, the damage caused by the thermal cycling is reduced to one fifth for the unloaded path, while the highly loaded paths undergo approximately three times more damage. It needs to be pointed out, that the capability of controlling the stress depends highly on the system design and the mission profile. With only small variations in the power, the thermal fluctuations can be completely eliminated from cells, while high fluctuations, such as in the presented case study affect all cells.

V. Experimental Validation

In the following, the electric measures of the multifrequency power routing are demonstrated and the capability of the imbalance power loading is validated on a laboratory prototype shown in Fig. 13. The dc-link voltage of the cells are adapted to generate an output voltage of 230 $V_{\rm rms}$ with the chosen ratio between dc-link voltage and grid voltage $V_{\rm grid}/V_{\rm DC} = 0.7$ and $V_{\rm grid}/V_{\rm DC} = 0.9$. In the setup, IXYB82N120C3H1 IGBTs are used. First, the transition between normal operation and multifrequency power routing is shown, before the output current spectrum is analyzed. Then, the power loading of the individual cells for application of the proposed method is validated.

A. Power Routing of the CHB Converter

The application requires a smooth transition between normal operation and the multifrequency power routing to ensure that the operation is not affected. The transition is demonstrated in Fig. 14, where a stepwise change is performed by showing the duty cycles of the cells and the output current. As expected from the simulation results, the current ripple is increasing. However, the transition is seamlessly conducted without any special technique, since the power routing is achieved by an open loop and the final reference ($v^* = v^*_A + v^*_B + v^*_C$) is always same regardless of the power routing as aforementioned.

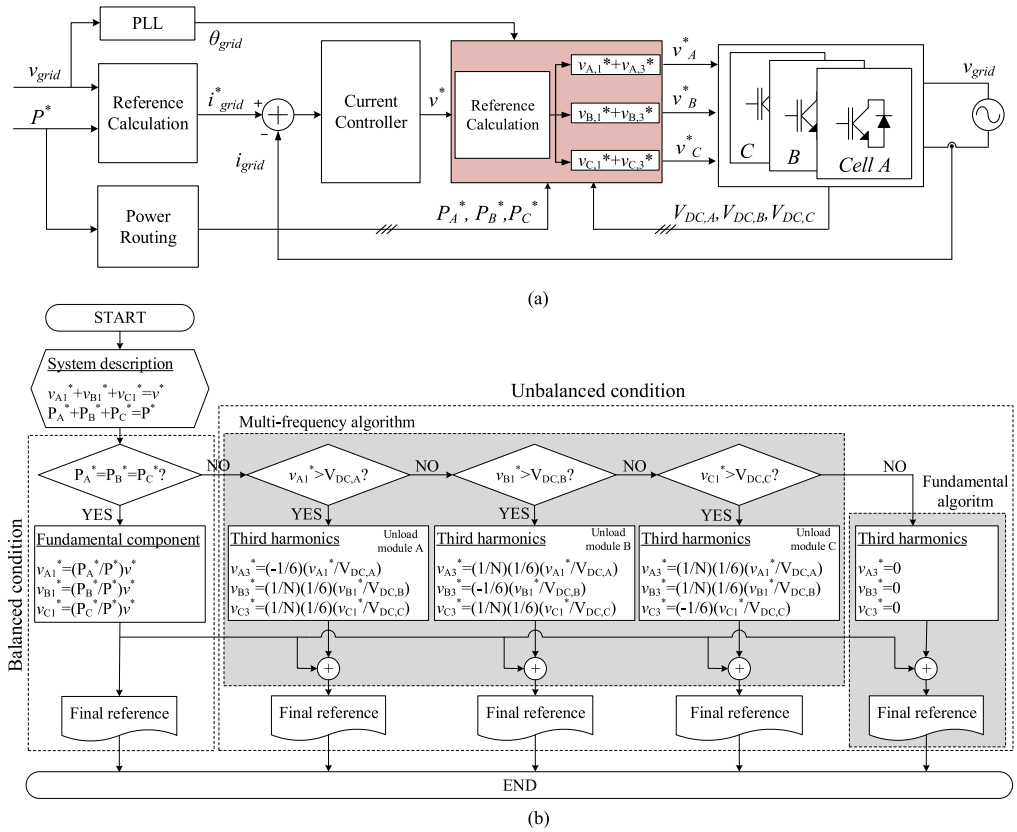

Fig. 11. (a) Control diagram including the power-routing algorithm and (b) flow chart to generate reconfigured references.

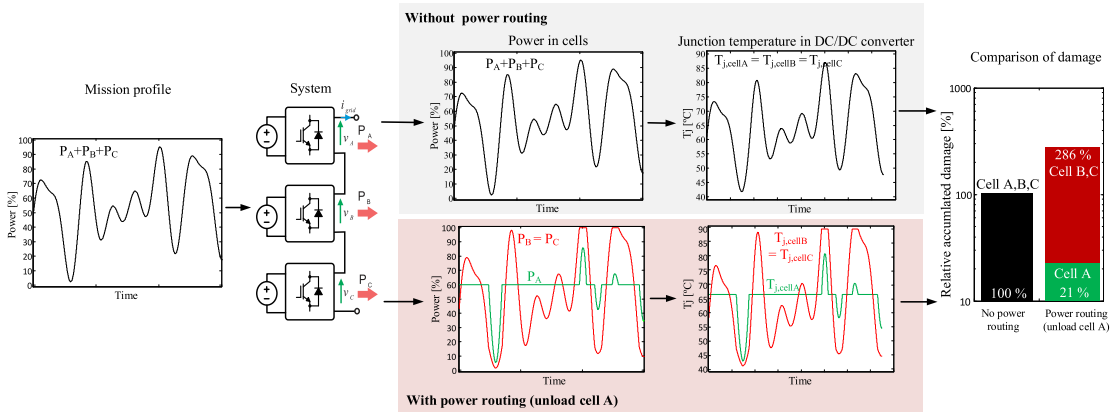

Fig. 12. Effect of power routing in the CHB converter on the thermal loading and the normed damage caused in the power semiconductors in the dc/dc converter with $V_{\mathrm{grid}}/V_{\mathrm{DC}} = 0.8$.

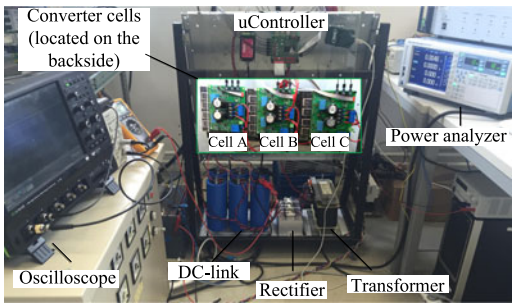

Fig. 13. Picture of the laboratory setup showing the seven-level CHB converter.

For analysis of the steady-state operation, Fig. 15 is presented. Similar to Fig. 4, it shows the duty cycles and the power distribution for three different cases. In the first case, Fig. 15(a) shows the similar loading of all devices, while Fig. 15(b) demonstrates the power routing with only the fundamental voltage and Fig. 15(c) the power routing with multifrequency method. Particularly interesting is the modulation index of cell C in all three configurations. For the chosen ratio between dc-link voltage and grid voltage, the capability to unload parts is already high, as in can be seen in case Fig. 15(b), where the modulation index of cell A and B is increased to its maximum, 1. The case in Fig. 15(c) demonstrates the increase of the modulation index in

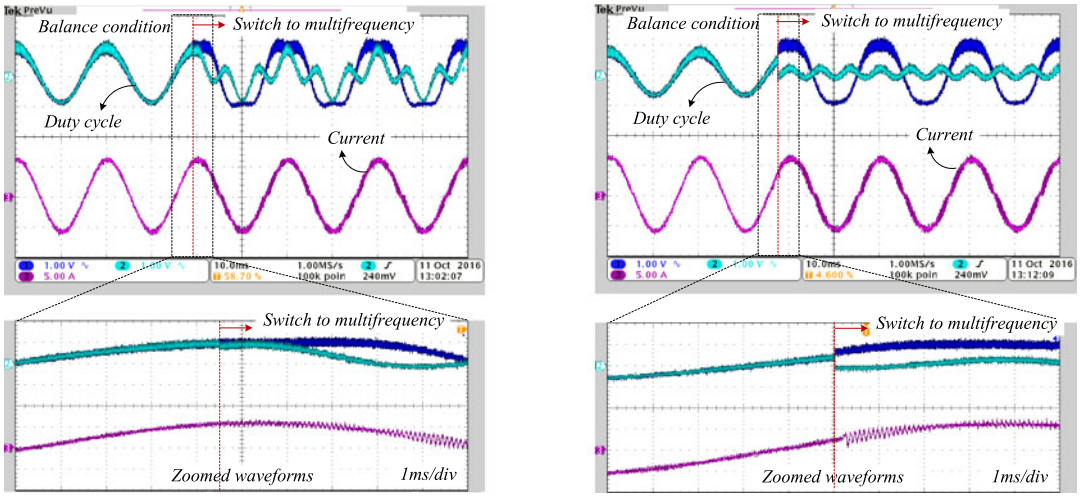

Fig. 14. Dynamic response of the activation of the multifrequency method for (a) $V_{\mathrm{grid}}/V_{\mathrm{DC}} = 0.9$ and (b) $V_{\mathrm{grid}}/V_{\mathrm{DC}} = 0.7$.

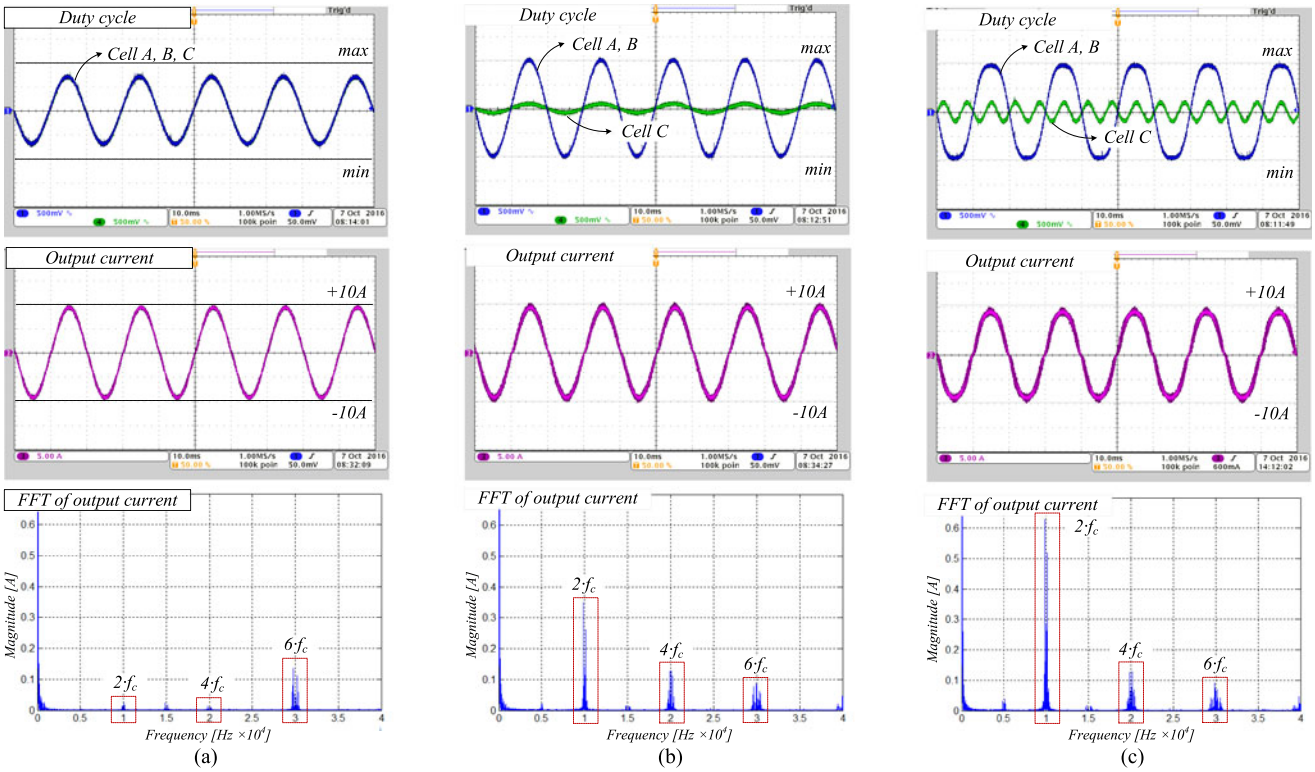

Fig. 15. Output current analysis in case of $V_{\mathrm{grid}}/V_{\mathrm{DC}} = 0.7$ showing the duty cycles, the output current and the current spectrum: (a) for balanced conditions, (b) unloading cell C with the fundamental voltage, and (c) unloading cell C by means of multifrequency method.

cell A and B to 1.05, while they are also processing 0.1 in the third-harmonic voltage. Therefore, cell C is not processing active power with the fundamental voltage, but exchanges reactive power with a modulation index of 0.2 in the third harmonic. The THD of the current is also matching very well the simulations by showing the increase of the second-harmonic component and the existence of the fourth-harmonic component during the power routing.

In case of lower voltage reserve ($V_{\mathrm{grid}}/V_{\mathrm{DC}} = 0.9$), the similar measurement case is shown in Fig. 16. The capability to unload a cell is limited, which is shown in Fig. 16(b), where the modulation index of cell C is 0.7, while the other cells are fully loaded. For the multifrequency power routing, cell A and B increase its overall maximum modulation index to 1.15 in the fundamental voltage and 0.17 in the third-harmonic voltage. This results for cell C in a modulation index of 0.4 in the

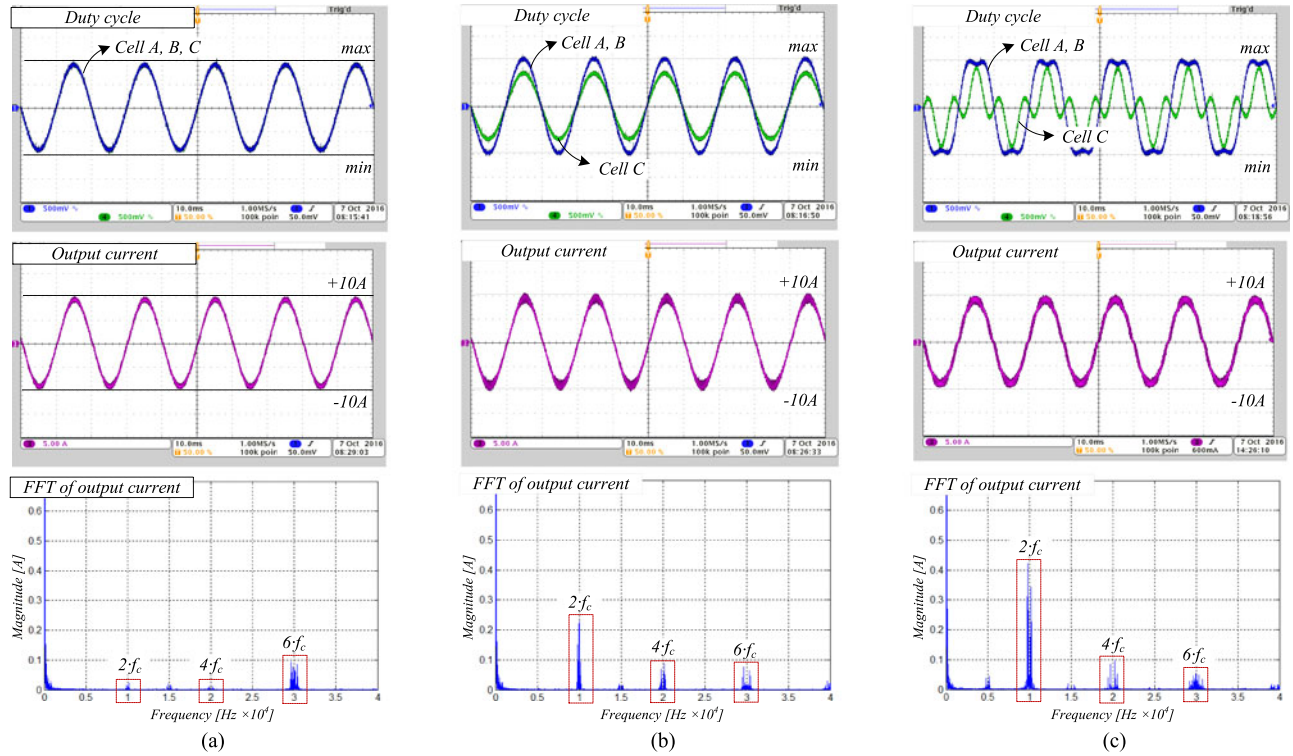

Fig. 16. Output current analysis in case of $V_{\rm grid}/V_{\rm DC} = 0.9$ showing the duty cycles, the output current and the current spectrum: (a) for balanced conditions, (b) unloading cell C with the fundamental component, and (c) unloading cell C by means of multifrequency method.

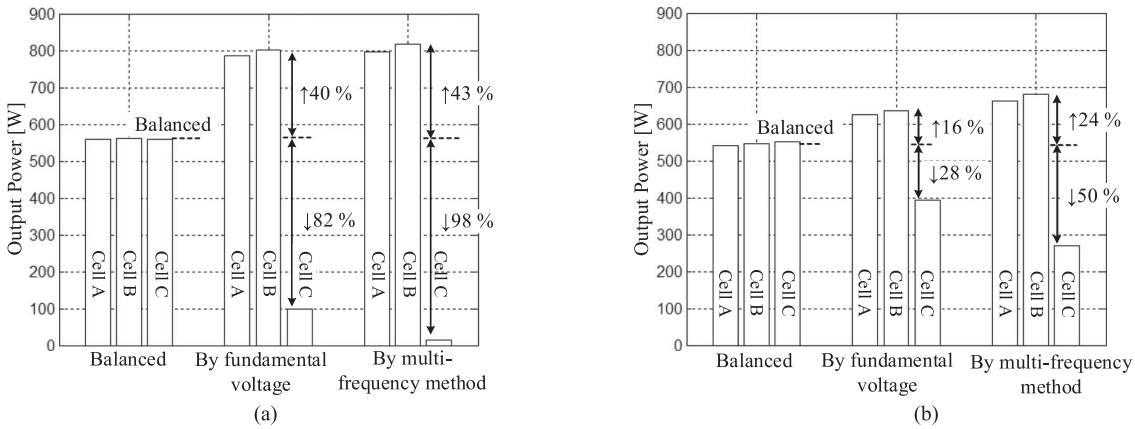

Fig. 17. Power measurement of each cell under balanced, unbalanced by fundamental and multifrequency. (a) $V_{\rm grid}/V_{\rm DC} = 0.7$ and (b) $V_{\rm grid}/V_{\rm DC} = 0.9$.

fundamental voltage and 0.34 in the third-harmonic voltage. As a consequence, the power path cannot be completely unloaded and still needs to process power in the dc/dc converter. Affected by the lower voltage reserve, the maximum power imbalance is limited and the increase of the current THD is lower than that for the case with $V_{\rm grid}/V_{\rm DC} = 0.7$. However, the trend is similar.

For the validation of the power loading of each cell, the power of the cells is measured by a power analyzer (Yokogawa WT1800) for the cases of Figs. 15 and 16. This is shown in Fig. 17. The power loading for an ratio $V_{\rm grid}/V_{\rm DC} = 0.7$ is shown in Fig. 17(a) and for $V_{\rm grid}/V_{\rm DC} = 0.9$, it is shown in Fig. 17(b). Similar to the waveforms shown before, the power is processed with equal loading, with the fundamental voltage method and with the multifrequency method. In accordance to the prior obtained results, the fundamental voltage enables to unload one device, while the capability is remarkably increased with the multifrequency method. In case of Fig. 17(a), the dc/dc converter of cell C is almost completely unloaded. However, it is required to contribute to the reactive power exchange with its third harmonic.

VI. Conclusion

This paper proposed to route the power in a CHB converter based on the condition of the components in connected power

paths. The loading of the converter cells is controlled to alter the power processed in the different paths and the multifrequency power routing using third harmonic has been proposed to improve the unbalanced power sharing between the cells. Moreover, power paths can be completely unloaded. The potential power-routing capability with third-harmonic component is analytically investigated and shown to improve the power-routing capability by more than 30% in comparison to the conventional method that uses only the fundamental voltage. It is demonstrated that an increased power imbalance affects a higher THD of the output current and redistributes the stress for the capacitors in the converter. In the opposite way to the power semiconductors, overloading a CHB cell reduces the stress for the capacitors, while unloading a cell increases the stress. The power-routing capability and its impact on the thermal stress of the power semiconductors is demonstrated with simulations, where the stress for power semiconductors in the unloaded power path was reduced to one-fifth under a mission profile with rapidly changing power. Measurements with a power analyzer on an experimental setup with a seven-level CHB converter validate the power-routing concept experimentally.

REFERENCES

[1] J. Rodriguez, S. Bernet, B. Wu, J. O. Pontt, and S. Kouro, "Multilevel voltage-source-converter topologies for industrial medium-voltage drives," *IEEE Trans. Ind. Electron.*, vol. 54, no. 6, pp. 2930–2945, Dec. 2007.

[2] Y. Li, Y. Wang, Y. Feng, J. Wu, and J. Liu, "Modeling and analysis of the cascaded H-bridge multilevel inverter using RMS feedback control," in *Proc. 2012 IEEE Energy Convers. Congr. Expo.*, Sep. 2012, pp. 3193–3198.

[3] X. She, A. Huang, and G. Wang, "3-D space modulation with voltage balancing capability for a cascaded seven-level converter in a solid-state transformer," *IEEE Trans. Power Electron.*, vol. 26, no. 12, pp. 3778–3789, Dec. 2011.

[4] S. Vazquez *et al.*, "Analysis of the power balance in the cells of a multilevel cascaded H-bridge converter," *IEEE Trans. Ind. Electron.*, vol. 57, no. 7, pp. 2287–2296, Jul. 2010.

[5] J. Ferreira, "Nestled secondary power loops in multilevel modular converters," in *Proc. IEEE 15th Workshop Control Model. Power Electron.*, Jun. 2014, pp. 1–9.

[6] J. Ferreira, "The multilevel modular DC converter," *IEEE Trans. Power Electron.*, vol. 28, no. 10, pp. 4460–4465, Oct. 2013.

[7] W. Song and A. Q. Huang, "Fault-tolerant design and control strategy for cascaded h-bridge multilevel converter-based STATCOM," *IEEE Trans. Ind. Electron.*, vol. 57, no. 8, pp. 2700–2708, Aug. 2010.

[8] N. Valentine, D. Das, B. Sood, and M. Pecht, "Failure analyses of modern power semiconductor switching devices," in *Proc. Int. Symp. Microelectron.*, vol. 2015, 2015, pp. 690–695.

[9] M. Liserre, M. Andresen, L. Costa, and G. Buticchi, "Power routing in modular smart transformers," *IEEE Ind. Electron. Mag.*, vol. 10, no. 3, pp. 43–53, Sep. 2016.

[10] P. Ghimire, A. R. de Vega, S. Beczkowski, B. Rannestad, S. Munk-Nielsen, and P. Thogersen, "Improving power converter reliability: Online monitoring of high-power IGBT modules," *IEEE Ind. Electron. Mag.*, vol. 8, no. 3, pp. 40–50, Sep. 2014.

[11] S. Yang, D. Xiang, A. Bryant, P. Mawby, L. Ran, and P. Tavner, "Condition monitoring for device reliability in power electronic converters: A review," *IEEE Trans. Power Electron.*, vol. 25, no. 11, pp. 2734–2752, Nov. 2010.

[12] H. Wang *et al.*, "Transitioning to physics-of-failure as a reliability driver in power electronics," *IEEE J. Emerg. Sel. Topics Power Electron.*, vol. 2, no. 1, pp. 97–114, Mar. 2014.

[13] S. Yang, A. Bryant, P. Mawby, D. Xiang, L. Ran, and P. Tavner, "An industry-based survey of reliability in power electronic converters," in *Proc. 2009 IEEE Energy Convers. Congr. Expo.*, Sep. 2009, pp. 3151–3157.

[14] M. Ciappa, "Selected failure mechanisms of modern power modules," *Microelectron. Reliab.*, vol. 42, no. 4, pp. 653–667, 2002.

[15] M. Held, P. Jacob, G. Nicoletti, P. Scacco, and M.-H. Poech, "Fast power cycling test of IGBT modules in traction application," in *Proc. 1997 Int. Conf. Power Electron. Drive Syst.*, vol. 1, pp. 425–430.

[16] H. Wang and F. Blaabjerg, "Reliability of capacitors for DC-link applications in power electronic converters—An overview," *IEEE Trans. Ind. Appl.*, vol. 50, no. 5, pp. 3569–3578, Sep.-Oct. 2014.

[17] M. Andresen, G. Buticchi, and M. Liserre, ''Study of reliability-efficiency tradeoff of active thermal control for power electronic systems," *Microelectron. Reliab.*, vol. 58, pp. 119–125, 2016.

[18] A. Dekka, B. Wu, N. R. Zargari, and R. L. Fuentes, "A space-vector PWM-based voltage-balancing approach with reduced current sensors for modular multilevel converter," *IEEE Trans. Ind. Electron.*, vol. 63, no. 5, pp. 2734–2745, May 2016.

[19] W. Li, L. A. Grégoire, and J. Bélanger, "A modular multilevel converter pulse generation and capacitor voltage balance method optimized for FPGA implementation," *IEEE Trans. Ind. Electron.*, vol. 62, no. 5, pp. 2859–2867, May 2015.

[20] D. G. Holmes and T. A. Lipo, *Pulse Width Modulation for Power Converters: Principles and Practice*, vol. 18, New York, NY, USA: Wiley, 2003.

[21] M. Moosavi, G. Farivar, H. Iman-Eini, and S. M. Shekarabi, "A voltage balancing strategy with extended operating region for cascaded h-bridge converters," *IEEE Trans. Power Electron.*, vol. 29, no. 9, pp. 5044–5053, Sep. 2014.

[22] L. Liu, H. Li, Y. Xue, and W. Liu, "Reactive power compensation and optimization strategy for grid-interactive cascaded photovoltaic systems," *IEEE Trans. Power Electron.*, vol. 30, no. 1, pp. 188–202, Jan. 2015.

[23] J. Chavarria, D. Biel, F. Guinjoan, C. Meza, and J. J. Negroni, "Energy-balance control of PV cascaded multilevel grid-connected inverters under level-shifted and phase-shifted PWMS," *IEEE Trans. Ind. Electron.*, vol. 60, no. 1, pp. 98–111, Jan. 2013.

[24] H. Jedtberg, A. Pigazo, M. Liserre, and G. Buticchi, "Analysis of the robustness of transformerless PV inverter topologies to the choice of power devices," *IEEE Trans. Power Electron.*, doi:10.1109/TPEL.2016.2612888.

[25] M. Andresen, M. Schloh, G. Buticchi, and M. Liserre, "Computational light junction temperature estimator for active thermal control," in *Proc. IEEE Energy Convers. Congr. Expo.*, 2016.

Youngjong Ko (S'16) received the B.Sc. and M.Sc. degrees from Ajou University, Suwon, South Korea, in 2009 and 2012, respectively, both in electronic engineering. Since 2015, he has been working toward the Ph.D. degree in electrical engineering at the University of Kiel, Kiel, Germany.

His research interests include grid-connected power converter and reliability in power electronics.

Markus Andresen (S'15) received the B.Sc. and M.Sc. degrees in electrical engineering and business administration from Christian-Albrechts-University of Kiel, Kiel, Germany. Since 2013, he has been working toward the Ph.D degree in electrical engineering in the Chair of Power Electronics, Christian-Albrechts-University of Kiel.

In 2010, he was an Intern in the Delta Shanghai Design Center, Delta Electronics (Shanghai) Co., Ltd., Shanghai, China. His research interests include control of power converters and reliability in power electronics.

Giampaolo Buticchi (S'10–M'13) was born in Parma, Italy, in 1985. He received the Master's degree in electronic engineering and the Ph.D. degree in information technologies from the University of Parma, Parma, Italy, in 2009 and 2013, respectively.

In 2012, he was Visiting Researcher at The University of Nottingham, Nottingham, U.K. He is currently a Postdoctoral Research Associate at the University of Kiel, Kiel, Germany. His research interests include power electronics for renewable energy systems, smart transformer-fed microgrids, and reliability in power electronics.

Marco Liserre (S'00–M'02–SM'07–F'13) received the MSc and PhD degree in Electrical Engineering from the Bari Polytechnic, respectively in 1998 and 2002. He has been Associate Professor at Bari Polytechnic and Professor in reliable power electronics at Aalborg University (Denmark). He is currently Full Professor and he holds the Chair of Power Electronics at Christian-Albrechts-University of Kiel (Germany).

Prof. Liserre was awarded with an European ERC Consolidator Grant, one of the most prestigious in Europe. He is a member of IAS, PELS, PES, and IES. He served all these societies in various capacities such as a Reviewer, Associate Editor, Editor, Conference, Chairman or Track Chairman. He has been the founding Editor-in-Chief of the IEEE INDUSTRIAL ELECTRONICS MAGAZINE, founding Chairman of the Technical Committee on Renewable Energy Systems, and the IES Vice-President responsible of the publications. He has received several IEEE awards.